ISIJ International, Vol. 31 (1991), No. 3, pp. 278-288

Comparison of Dynamic Recrystallization and Conventional Controlled Rolling Schedules by Laboratory Simulation

L.N. PUSSEGODA[1] and J.J. JONAS

Department of Metallurgical Engineering, McGill University, Montreal, Quebec, Canada H3A 2A7. 1) McGill University. Now at Fleet Technology, Kanata, Ontario, Canada K2K 1Z8.

(Received on July 23, 1990; accepted in the final form on September 14, 1990)

A seamless tube mill rolling process was simulated with the aim of optimizing the ferrite grain refinement by decreasing the finish rolling temperature during the stretch reducing mill (SRM) stage. Tests were performed on one Nb–V and two Ti–V micralloyed steels. For the Ti–V steels, maximum grain refinement is achieved when the SRM exit temperature is just above the A_{r3}; at a cooling rate of 3.5°C/s during transformation, ferrite ASTM grain size numbers of #13 and higher are produced. When the reductions are applied below the no-recrystallization temperature or T_{nr}, the strains are accumulated at first as a result of the absence of static recrystallization during the short interpass times. At larger strains, *dynamic* recrystallization is initiated, due to the absence of strain-induced precipitation during the brief unloading intervals. Under these conditions, the rolling loads are lower than when a conventional controlled rolling schedule is employed. In the latter case, the interpass times are sufficiently long for the occurrence of appreciable strain-induced precipitation, which is responsible for the prevention of dynamic recrystallization, and the consequent accumulation of strain and pancaking of the austenite. For the Nb–V steels, when the SRM cooling curve passes through the nose of the CCP (continuous-cooling-precipitation) P_S curve, austenite pancaking takes place. By contrast, when the cooling curve passes *above* or *below* the CCP curve, the dynamic recrystallization of austenite is initiated, leading to ferrite grain sizes which are generally finer than those produced by the pancaking process.

KEY WORDS: dynamic recrystallization; recrystallization controlled rolling; conventional controlled rolling; austenite and ferrite grain refinement; strain induced precipitation; hot strength; laboratory simulation.

1. Introduction

In conventional steel rolling, ferrite grain refinement can be produced by recrystallization controlled rolling (RCR) when reductions are carried out above the "no-recrystallization temperature" (T_{nr}) or by "pancaking" the austenite prior to the austenite-to-ferrite transformation (CCR or conventional controlled rolling) when finish rolling is performed below the T_{nr}.[1,2] More recently, a third type of controlled rolling has been developed,[3–5] which is referred to here as DRCR or dynamic recrystallization controlled rolling. It relies on the initiation of *dynamic* recrystallization during deformation as opposed to *static* recrystallization during the interpass delays, as in typical RCR processes. DRCR can produce more effective refinement than either of the two preceding methods.

The present work was done in order to determine methods of optimizing ferrite grain refinement by DRCR processing. Earlier work on Ti–V steels indicated that dynamic recrystallization takes place during finish rolling in the stretch reducing mill (SRM) of a seamless tube making process. This is because the interpass times were too short to permit static recrystallization between mill stands at low rolling temperatures, leading to the accumulation of strain.[5] In a similar way, during laboratory simulation of strip mill rolling, the application of sufficient strain *below* the T_{nr} again produced dynamic recrystallization. In this case, when the lowest possible finishing temperatures were employed, ferrite grain sizes finer than ASTM #13 were produced.[4]

The tube mill schedules described above, however, had not been optimized from a grain refinement point of view, which would have required the use of lower finishing temperatures and the application of all of the SRM strain below the T_{nr}. Simulations were therefore carried out in which the full SRM strain was applied below the T_{nr}, and the SRM rolling temperatures were further reduced so that the last pass was applied just above the A_{r3}. Simplified plate schedules covering the same temperature range were also simulated, so that the resistances to hot deformation for the two type of schedules, *i.e.*, DRCR and CCR, could be compared. Two types of microalloyed steels were studied:

i) two Ti–V grades, designed for RCR processing[5,6]; and
ii) a Nb–V grade, designed for the pancaking of austenite during plate rolling.

2. Experimental Procedure

2.1. Test Schedules

The schedules were simulated by means of torsion testing, a method which has been employed successfully for investigating reversing,[7,8] and strip mill

schedules,[3,4,9] as well as seamless tube piercing and rolling.[5] For the simulation of plate rolling and the determination of T_{nr}, a simplified average schedule was employed (Fig. 1).[7] During test execution, the temperature was decreased from the reheat temperature of 1 250 to 600°C at a mean rate of 1°C/s.

The critical pass parameters of strain and strain rate during tube piercing and rolling were determined earlier and converted into test schedules, following a method presented in more detail elsewhere.[10] The specific rolling schedule depends primarily on the final tube size. A typical schedule representing a small tube size, in which sufficient SRM strain is applied to produce dynamic recrystallization,[5] is presented in Table 1. The schedule can be clearly divided into two temperature regions. The piercing and multi-pipe mill (MPM) stages (passes 1 to 6) are carried out at high temperatures (roughing), while the SRM deformation (passes 7 to 22) is applied at lower temperatures (finishing). In the present investigation, the specimens were cooled to about 950°C before being reheated to 1 000°C, to simulate the tube reheat furnace. The finish rolling (SRM) stage was carried out at a series of temperatures, the lowest of which led to an SRM exit temperature of 735°C, which is about 20°C above the A_{r3}. This was done by allowing the specimens to cool from the tube furnace temperature of 1 000°C to lower temperatures at 1°C/s, before entry into the SRM. During the simulation of SRM rolling, average cooling rates of 6 to 8°C/s were applied by turning off the radiant furnace associated with the torsion machine.* The cooling rate *after* the SRM (*i.e.*, during the austenite-to-ferrite transformation) was about 3.5°C/s.

In order to compare the SRM (finish rolling) part of the simulation with a typical reversing mill schedule, the following approach was adopted:

(1) Roughing was identical to the piercing and MPM stages.

(2) Finishing was represented by 8 passes, each of 0.2 strain; *i.e.*, a total strain of 1.6 was applied (identical to the SRM strain), with interpass delays of 20 s. The passes were given in the same temperature range by employing a much slower cooling rate than for the SRM simulations.

The cooling rate during the austenite-to-ferrite transformation was maintained, as before, at about 3.5°C/s.

2.2. *Materials and Testing Procedure*

The compositions of the materials tested are given in Table 2. The Ti–V steels, supplied by the Metals Technology Laboratories, CANMET, were laboratory cast in permanent iron molds of section size 125 mm × 150 mm. The Ti, V and N levels were based on alloys designed for RCR processing.[6] The Nb–V steel was supplied by the Algoma Steel Corporation in plate form in a chemistry designed for austenite pancaking during plate rolling. Specimens of gauge length 20 mm and diameter 6.4 mm were subjected to multi-stage torsion tests, conducted in an argon atmosphere, using the schedules described above. The torsion testing equipment and methods have been described elsewhere.[11]

Table 1. S simulation.

Pass #-Type of mill	Equivalent strain per pass	Temperature (°C)	Delay time between passes (s)
1-piercer	1.60	1 230	54
2-MPM	0.45	1 085	1
3-MPM	0.40	1 072	1
4-MPM	0.30	1 060	0.5
5-MPM	0.20	1 050	0.5
6-MPM	0.18	1 020	75
Tube reheat furnace	—	1 000	5
7 to 22-SRM	0.10	1 000 to 860	0.5

Note: Soaking temperature: 1 250°C for 15 min
Delay time between billet reheating furnace and piercer: 80 s
Time in intermediate (tube) reheat furnace: 10 min
The strain rate: 2 s^{-1} for each pass
The average cooling rate during finish rolling: ~8°C/s

Table 2. Chemical composition of the steels. (wt%)

Element	Steel grades		
	10C-01Ti-10V	19C-01Ti-15V	10C-03Nb-04V
C	0.10	0.19	0.10
Si	0.30	0.36	0.24
Mn	1.70	1.70	1.26
S	0.008	0.008	0.01
P	0.013	0.014	0.01
Al	0.014	0.027	0.042
V	0.10	0.15	0.04
Ti	0.010	0.012	—
N	0.0150	0.0185	0.0085
Nb	—	—	0.027

The simulation specimens were polished and etched with 2 % nital to reveal the final microstructure on tangential planes just below the surface. The ferrite grain sizes were determined by the intercept method. In order to study the development of the austenite microstructure during the SRM stage of rolling, specimens were quenched at selected stages of the simulations. The austenite grain size was revealed by etching for about 40 s in a saturated aqueous picric acid solution containing HCl and Teepol heated to about 80°C.

3. Results

3.1. *Determination of the No-recrystallization Temperature or* T_{nr}

Laboratory torsion testing can also be used for the determination of the recrystallization stop temperature or T_{nr}.[7,12] For this purpose, the simplified average plate schedule was employed. The von Mises

* The cooling rates for SRM entry temperatures of 1 000 and 840°C were 8 and 6°C/s, respectively, with intermediate cooling rates being employed at the intermediate entry temperatures.

equivalent stress–strain curves were derived from the torque–twist data,[13] from which the mean flow stress (MFS) for each pass was calculated by numerical integration.[5]

The T_{nr} can be determined from the variation of the MFS with absolute inverse pass temperature. This is made relatively straight forward through the use of the average schedule, in which all the hot rolling parameters are kept constant except the temperature.[7,12] In the high temperature region, the austenite undergoes *static* recrystallization between mill passes, as a result of which the grain size is refined and the work hardening or ' strain ' accumulated within the roll pass is eliminated. Thus there is a low rate of increase of MFS with inverse pass temperature and the slope is typical of RCR rolling (Fig. 1). In the vicinity of the T_{nr}, there is a transition to a higher rate of flow stress increase with temperature decrease. This is a result of the change from the recrystallization to the no-recrystallization behavior; the higher stress levels are thus due to the strain accumulation which is associated with pancaking of the austenite grains.[3,7,12] Pancaking cannot be achieved successfully unless strain-induced carbonitride precipitates are produced in the austenite during the interstand intervals in sufficiently copious quantities.[14,15] Because of the relative sluggishness of such precipitation, this usually requires interpass delays of 10 s or more. Thus, the slope displayed by the MFS *vs.* $1/T$ curve *below* the T_{nr} is representative of pancaking and of CCR.

From Fig. 1(a), it can be seen that the T_{nr} is 940°C in the 19C–01Ti–15V grade Ti–V steel; this is about 150°C below the equilibrium solution temperature of VN, which is 1 091°C.[5] The T_{nr} for the 10C–03Nb–04V grade Nb–V steel can be determined from Fig. 1(b) as 980°C. According to equilibrium solubility data,[16] the Nb(CN) solution temperature in the Nb–V steel is 1 137°C, and thus the difference is again approximately 150°C.

3.2. *Comparison of DRCR and CCR in the Same Temperature Range*

The MFS values determined from the unmodified SRM schedule (Table 1) are presented in Fig. 2, together with those of the simplified reversing mill schedule. For the 10C–01Ti–10V grade, 8 of the SRM passes were applied above the T_{nr}; thus the grain refinement that can be produced by DRCR was not optimized in this case.[4] Also indicated in Fig. 2 are the slopes representing the MFS *vs.* inverse pass temperature behaviors for the RCR, CCR, and DRCR processes.[3,5] In the Ti–V steels, the early stages of strain accumulation (during the first 4 passes) are followed by dynamic recrystallization during the remaining 12 passes of the SRM schedule, as indicated by the DRCR slope.[5]

The plate schedule, on the other hand, displays an average rate of flow stress increase during the passes applied above the T_{nr}, which is similar to the RCR slope, indicating full static recrystallization. As the temperature is decreased below the T_{nr}, however, there is a transition to a higher rate of flow stress increase with inverse temperature, to a value comparable with the pancaking slope. Thus, below the T_{nr}, the plate schedule displays an MFS behavior indicative of austenite pancaking, whereas the flow stress characteristics of the SRM schedule are consistent

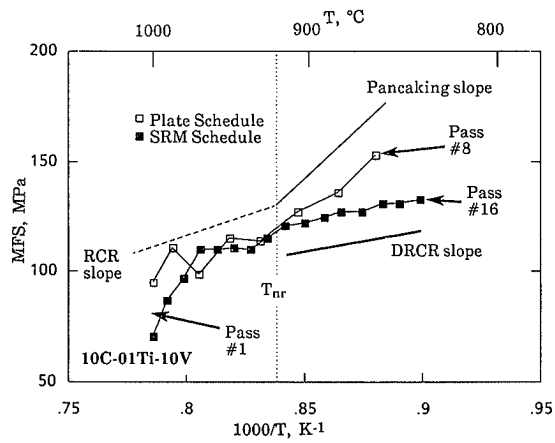

Fig. 2. MFS values for the 10C–01Ti–10V steel deformed according to the unmodified SRM schedule (0.5 s interpass delays) and the plate schedule (20 s interpass delays).
Note that the total strain applied (1.6) is the same in the two schedules.
Typical *slopes* associated with RCR, DRCR and CCR rollings[3–5] are also indicated.
Note that the MFS scale begins at 50 MPa.

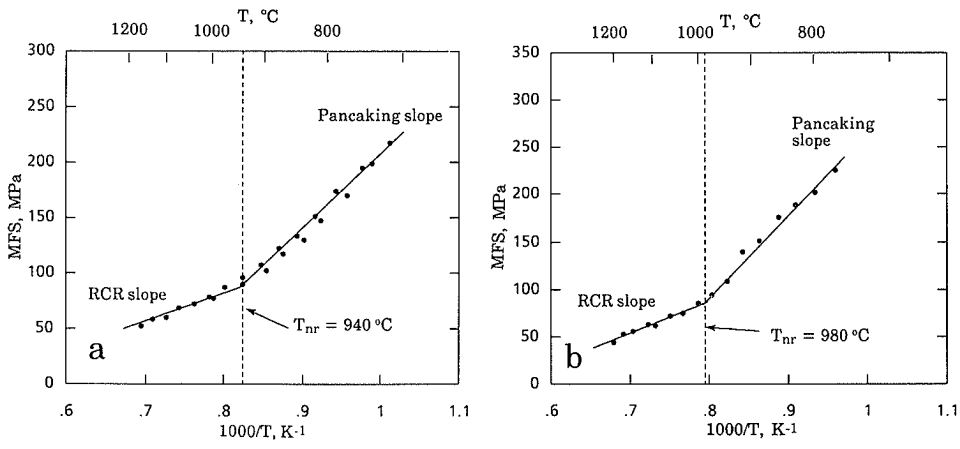

Fig. 1.
Determination of the T_{nr} from the dependence of MFS on inverse pass temperature for a simplified schedule representing a plate or reversing mill. (a) 19C–01Ti–15V grade and (b) 10C–03Nb–04V grade
A schedule consisting of 17 passes, each of 0.2 equivalent strain, with 30 s interpass delays at a strain rate of 2 s^{-1} was employed.[7]
The cooling rate was 1°C/s.

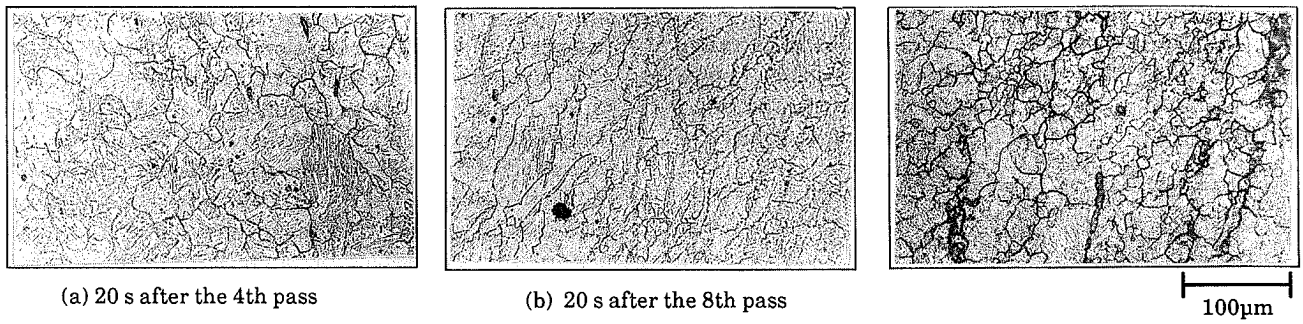

(a) 20 s after the 4th pass (b) 20 s after the 8th pass (c) after (within 3 s of) the 16th pass

Fig. 3. Austenite microstructures in the Ti–V grade: (a), (b) for the plate schedule, and (c) for the SRM simulation.

with the occurrence of dynamic recrystallization. This analysis is confirmed by the austenite microstructures presented in Fig. 3, which have the following features:

(1) Just before the 5th pass (above the T_{nr}), a fully recrystallized structure is displayed (Fig. 3(a)). However, evidence that strain accumulation (pancaking) is taking place during the 3 passes (to a strain of 0.6) applied below the T_{nr} is presented in Fig. 3(b).

(2) Fig. 3(c) illustrates the fully recrystallized structure present about 3 s after the 16th pass, confirming that dynamic and metadynamic recrystallization are occurring in the SRM schedule.

In the above comparison, the important difference between the two simulations is the total time elapsed below the T_{nr} after the commencement of straining; for the reversing mill simulation, this is more than 40 s, while for the SRM simulation, this period is 7 s. Thus, for the reversing mill schedule, there is sufficient time for the copious precipitation of VN to take place which is responsible for pancaking, whereas, in the SRM simulation, there is insufficient time for more than a limited amount of precipitation.

The flow stress data for the modified SRM simulation *where the total strain is applied below the* T_{nr}, are presented in Fig. 4 for the 19C–01Ti–15V grade. The MFS values show that strain accumulation is taking place during the first 5 passes, followed by dynamic recrystallization, as indicated by the DRCR slope. By contrast, in the plate simulation, the early stages of strain accumulation are *not* followed by the initiation of dynamic recrystallization, as indicated by the pancaking slope. It is clear from this comparison that the resistance to hot deformation is about 30 % greater for the plate schedule. This is attributable to the continuous strain accumulation that takes place in the plate schedule coupled with the occurrence of dynamic recrystallization in the SRM schedule.

In Fig. 5(a), the flow curves representing the modified SRM simulation are displayed after *replotting* at a constant ' standardized ' temperature of 865°C, using the method described earlier; these envelope shows the ' single peak ' behavior characteristic of the grain refinement type of dynamic recrystallization.[5] The ' rounding ' of the flow curves (during loading) pertaining to the individual passes (beyond the 3rd pass) is due to static recovery and/or post-dynamic recrystallization.[17] Note, however, that due to the short

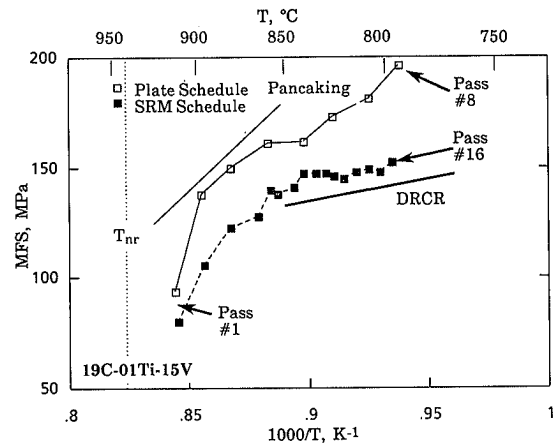

Fig. 4. Mean flow stress *vs.* inverse pass temperature for the modified SRM schedule (total strain applied below the T_{nr}) compared with the plate schedule.
Note that the total strain applied (1.6) is the same in both schedules.
Typical pancaking and DRCR *slopes*[3–5] are shown for reference.
Note also that the MFS scale begins at 50 MPa.

interpass times (0.5 s), there is only limited softening produced by these processes.

The austenite grain structures present at three successive stages of the modified SRM simulation are illustrated in Fig. 5(b); the following observations can be made about these microstructures:

(1) The structure after the 4th pass is representative of a strain accumulation of 40 %.

(2) Within 3 s of the 9th pass (curve 2 in Fig. 5(a)), *i.e.*, somewhat beyond the ' peak strain ', many of the pancaked grains have been replaced by fine dynamically and metadynamically recrystallized austenite grains. Note, however, that some pancaked grains are still present (P).

(3) At the end of the SRM deformation, *i.e.*, after the 16th pass, dynamic recrystallization has penetrated right into the centers of the pancaked grains.

The above observations confirm that when the full SRM strain is applied below the T_{nr}, the short interval between passes (0.5 s) is insufficient for the strain-induced precipitation of VN to occur in sufficient quantities to prevent the initiation of dynamic recrystallization. By contrast, when the 20 s interpass delays of the plate simulation were employed, there was sufficient VN precipitation to prevent both static and

dynamic recrystallization.

An interesting feature of this interpass time range (0.5 to 20 s) is that the MFS's *increase* with the length of the unloading period. This is opposite to the trend observed in plain C steels, where the flow stresses in subsequent passes *decrease* as the time available for recovery and recrystallization is increased! However, this effect is *not* a direct consequence of precipitation hardening, the precipitates generally being too coarse for this purpose. Rather, it is due to the stabilization of the work hardened substructure by strain-induced precipitation when long interpass times are used and its inability to resist dynamic recrystallization in the absence of precipitation (short interpass times).

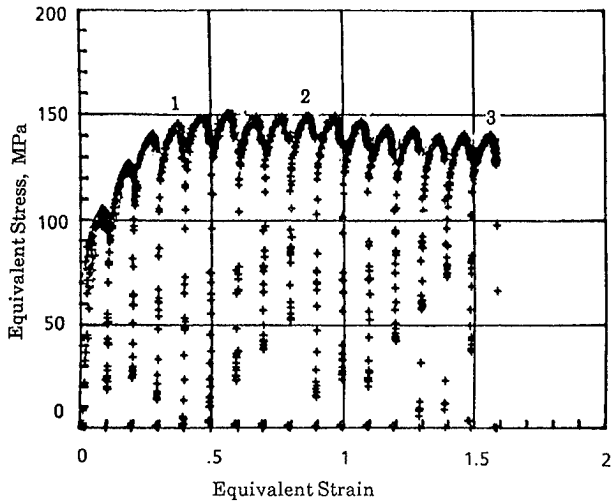

Fig. 5(a). SRM flow curves for the 19C–01Ti–15V steel, corrected to a constant ' standardized ' temperature of 865°C, using the method described earlier.[5]
Here the total SRM strain is applied below the T_{nr}. Note that the flow curve envelope displays the ' single peak ' behavior characteristic of dynamic recrystallization.

3.3. *Resistance to Hot Deformation in the SRM*

Some tests were carried out where the SRM entry temperature was reduced while maintaining the reheat furnace temperature at a fixed value of 1 000°C. The MFS values produced during these simulations are presented in Figs. 6(a) and 6(b) for the 0.10 and 0.15 % V steels, respectively. At the highest SRM entry temperature of 1 000°C, there is strain accumulation during the first few passes, leading to the initiation of dynamic recrystallization, as indicated by the change in the rate of increase of the MFS with inverse pass temperature. When the SRM entry temperature was reduced to 910°C and then to 850°C, the initiation of dynamic recrystallization was delayed to later and later passes, as indicated by the higher stress levels at which the changeover to the DRCR slope occurs.

The above observations are in agreement with some recent simulations of strip rolling, where progressively

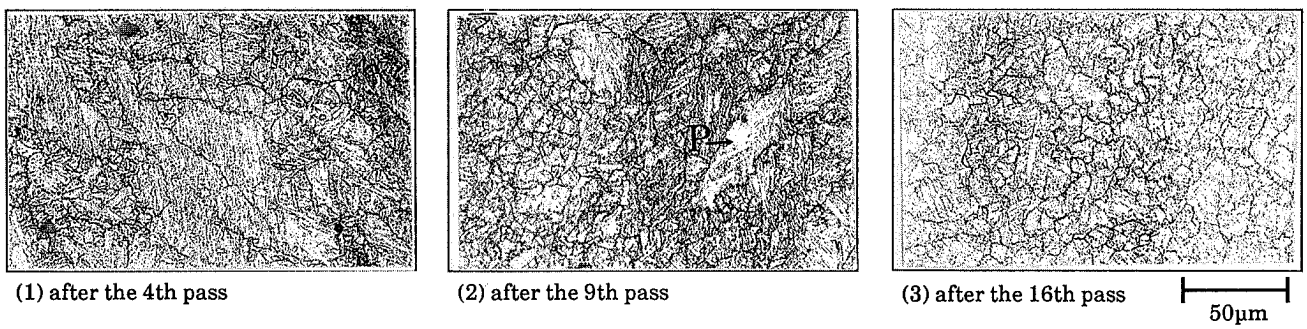

Fig. 5(b). Development of austenite microstructure during modified SRM rolling below the T_{nr}; the samples were quenched after the passes identified as 1, 2 and 3 in Fig. 5(a).

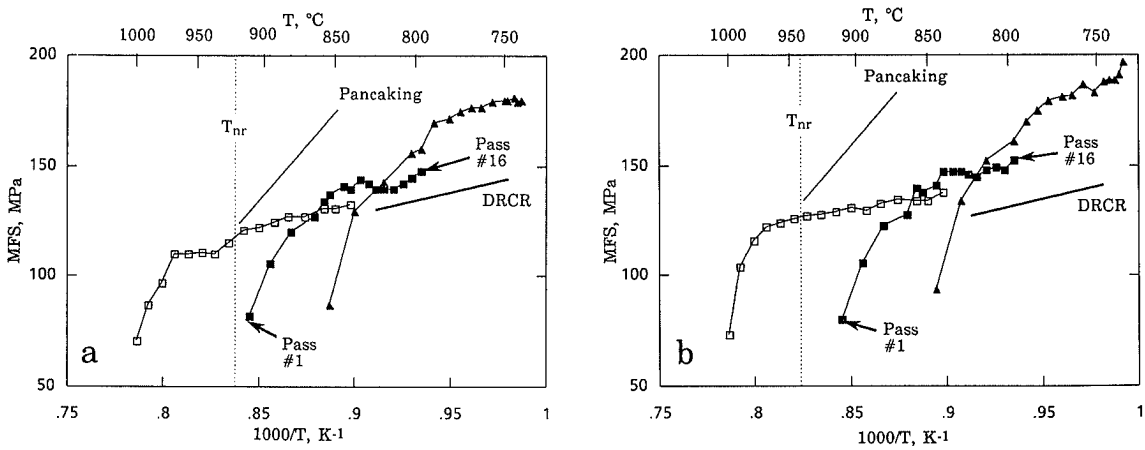

Fig. 6. Dependence of mean flow stress on inverse pass temperature for the SRM simulations carried out on the (a) 10C–01Ti–10V, and (b) 19C–01Ti–15V grades.
Typical DRCR and pancaking *slopes* are shown for reference.
Note that the MFS scale begins at 50 MPa.

higher stress levels were required to initiate dynamic recrystallization as the finish rolling temperature was decreased.[3,4] They are also consistent with the dynamic recrystallization behavior of plain C and HSLA steels during isothermal, constant strain rate testing; decreasing the test temperature delays the onset of dynamic recrystallization by increasing the ' peak strain ' and thus the peak stress.[18,19]

The increase in the stress level at which the changeover to the DRCR slope occurs is small when the SRM entry temperature is decreased from above to below the T_{nr} (compare the open and full square data points, respectively). By contrast, when the reduction in the SRM entry temperature is smaller (60°C compared to 90°C in the former case) but entirely below the T_{nr}, a relatively large increase in the stress level necessary to initiate dynamic recrystallization is produced (compare the full square and triangular data points). In the more highly alloyed steel (Fig. 6(b)), there is some strain accumulation during the last few passes, where the rate of flow stress increase is clearly greater than the DRCR slope. This can be attributed to the strain-induced precipitation of VN in copious quantities at this stage of rolling. This observation is considered in more detail in the Discussion section.

3.4. *Optimization of Ferrite Grain Refinement by DRCR*

The effect on grain refinement of decreasing the SRM entry and exit temperatures is displayed in Fig. 7. In this case, the lowest SRM exit temperature of 735°C is about 20°C above the A_{r3} for ' conditioned austenite ' of this steel.[20] It is clear from this figure that a reduction in the finishing temperature produces significant austenite grain refinement. All the austenite microstructures (Figs. 7(a) through 7(c)) at the exit of the SRM are dynamically recrystallized, and the lowest exit temperature of 735°C is at about the limit of the grain refinement that can be produced by the DRCR process in this case. A further reduction in the temperature would cause pancaking, as the last couple of passes at about 735°C produce the strain accumulation described above. The room temperature microstructures corresponding to the austenite structures are shown in Figs. 7(d) through 7(f), and confirm that the austenite grain refinement is translated into ferrite grain refinement.[1]

The austenite and corresponding ferrite grain sizes of the microstructures presented in Fig. 7 are plotted against the SRM exit temperature in Fig. 8. This figure shows that lowering the exit temperature from 860 to 735°C produces a decrease in the austenite grain size from 14 to 6 μm, and a corresponding decrease in the ferrite grain size from 6.6 to 3.3 μm. The finest ferrite grain size is equivalent to ASTM #13, and is similar to the smallest sizes produced in the strip mill simulation.[4] Also illustrated in this figure is the ferrite grain refinement obtained by decreasing the SRM exit temperature from 860 to 740°C for the 10C–01Ti–10V grade. In this case, the ferrite

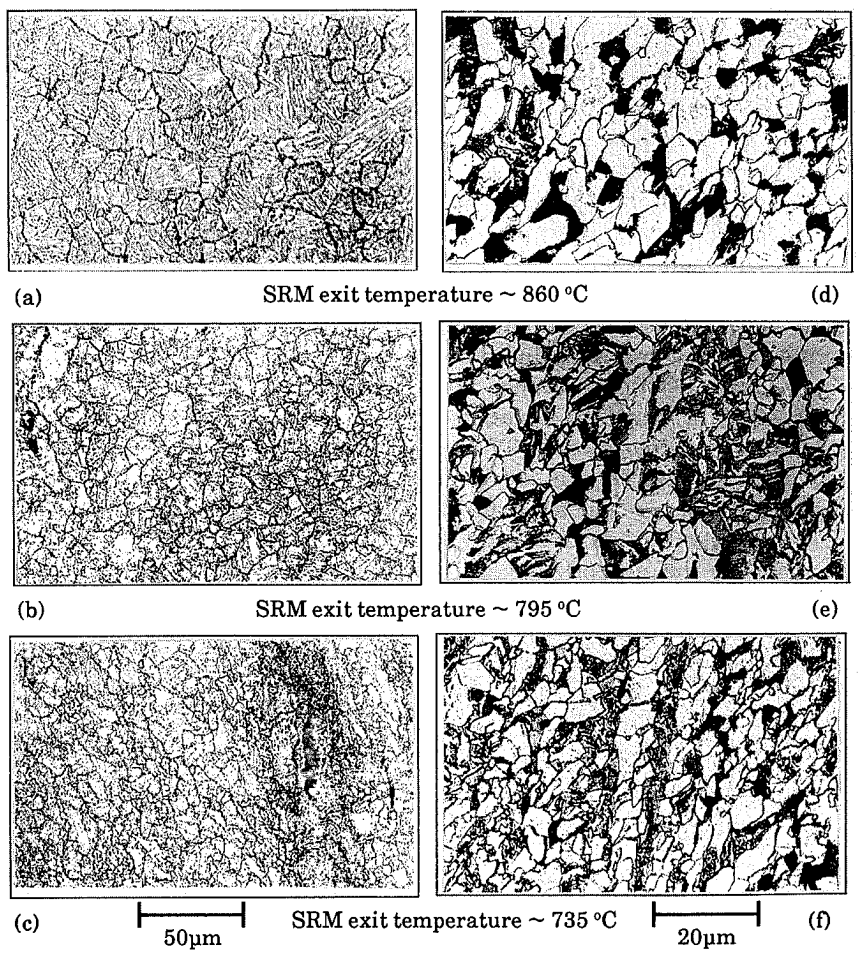

Fig. 7.
Austenite microstructures (a) to (c), after the SRM simulations of Fig. 6(b), and the corresponding room temperature microstructures (d) to (f).
Note that significant grain refinement is produced by decreasing the finish rolling temperature from 860 to 735°C.

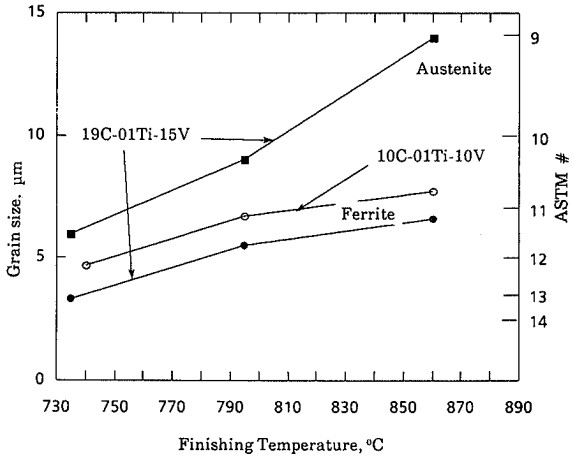

Fig. 8. Grain refinement produced by decreasing the SRM exit temperature.
The cooling rate during the austenite-to-ferrite transformation was about 3.5°C/s.

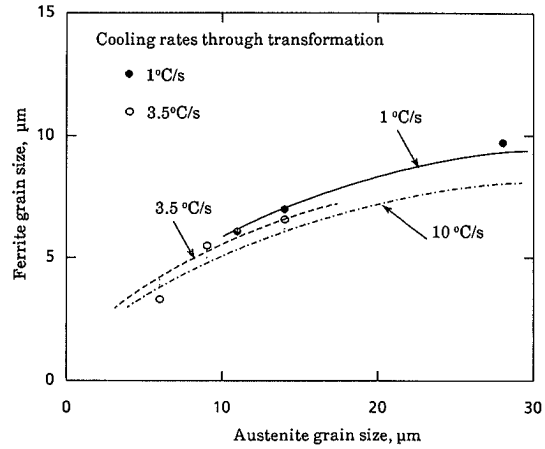

Fig. 9. Relationship between the austenite and ferrite grain sizes, for increasing cooling rates through the transformation.
The open data points for the 19C–01Ti–15V steel correspond to the experimental results shown in Fig. 8; the full points are from earlier work.[5,20]
The three curves represent the ferrite grain sizes predicted according to the empirical equation of Siwecki[21] with constants D and E modified for the higher C content of this steel.

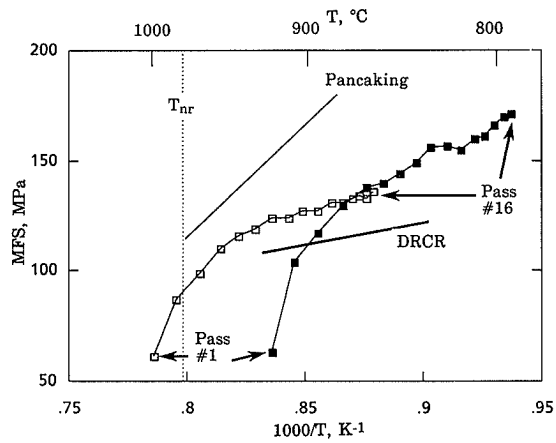

Fig. 10. Dependence of the mean flow stress on inverse pass temperature for the SRM simulations carried out on the 10C–03Nn–04V steel.
Typical DRCR and pancaking *slopes* are shown for reference.
Note that the MFS scale begins at 50 MPa.

grain size decreased from 7.7 to 4.7 μm; thus, the ferrite grain sizes are larger in this less alloyed material than in the 19C–01Ti–15V grade. This can be attributed to two factors:

(1) The 10C–01Ti–10V grade, with less C in solution in the austenite, has a higher A_{r3} temperature, which decreases the austenite-to-ferrite grain size ratio.[21]

(2) In the 10C–01Ti–10V grade, the growth of the ferrite during transformation is less restricted due to the smaller volume fraction of the non-ferritic phase.[5]

In Fig. 9, the relationship between the austenite and the corresponding ferrite grain sizes is displayed for the 19C–01Ti–15V grade. The open points represent the data from Fig. 8, and the full symbols are from earlier results.[5,20] The curves represent an equation taken from the literature[21] and corrected for the higher C content of the present steel, which relates the austenite and ferrite grain sizes to the cooling rate during transformation. This relation is applicable to Ti–V microalloyed steels containing ~0.01 % Ti and to the austenite grains produced by *static* recrystallization, *i.e.*, by RCR processing. It is clear from this figure that the empirical equation fits the experimental data for cooling rates of 3.5 and 1°C/s, except for the finest grain size. In the latter case, the actual ferrite grain size is smaller than the predicted value. This supports the view that some strain accumulation is present in the austenite microstructure displayed in Fig. 7(c), and that this strain produces additional ferrite grain refinement, as called for by the microstructure model of Sellars and Beynon.[22] The grain refinement produced by increasing the cooling rate through the transformation is small, according to Fig. 9, in agreement with earlier results for the 19C–01Ti–15V grade.[5]

3.5. *SRM Simulation Employed on the* Nb–V *Steel*

The MFS values obtained during simulated SRM rolling of the Nb–V steel are displayed in Fig. 10. Two SRM entry temperatures were investigated:

1) The unmodified SRM schedule, where the entry temperature is 1 000°C.
2) A modified SRM schedule, where the entry temperature is reduced to 910°C.

The unmodified SRM schedule, where the entry temperature is *above* the T_{nr} (determined from Fig. 1(b)) produces strain accumulation up to about the 7th pass, as indicated by a rate of MFS increase with inverse pass temperature similar to the pancaking slope. It is clear that beyond the 7th pass, the rate decreases and approaches the DRCR slope. This behavior is similar to that observed in the Ti–V steels and presented above.

By contrast, when the SRM entry temperature is lowered to 910°C, *i.e.*, to 70°C *below* the T_{nr}, the flow

stress data reveal that strain accumulation continues to take place up to the exit of the SRM. This behavior indicates that, *in this specific case*, sufficient strain-induced precipitation is taking place to produce austenite pancaking. In Fig. 11, the flow curves representing the modified SRM simulation are displayed after *replotting* at a constant ' standardized ' temperature of 860°C. The envelope of these flow curves *does not* display the ' single peak ' behavior characteristic of dynamic recrystallization.

The effect on the austenite and ferrite microstructures of decreasing the SRM entry and exit temperatures is illustrated in Fig. 12. It is clear from this figure that reducing the entry temperature produces pancaking of the austenite grains. The pancaked grains are quite coarse because of the absence, in the

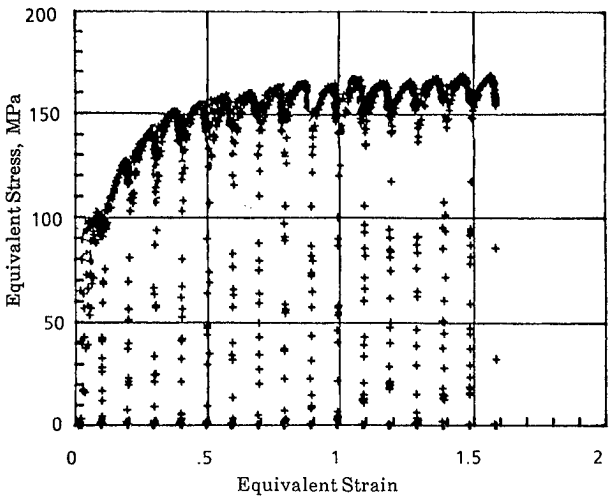

Fig. 11. SRM flow curves for the 10C–03Nb–04V steel, corrected to a constant ' standardized ' temperature of 860°C, using the method described earlier.[5] Here the SRM entry and exit temperatures are 70 and 194°C below the T_{nr}, respectively.
Note that the flow curve envelope *does not* display the ' single peak ' behavior characteristic of dynamic recrystallization.

Nb–V steel, of the fine TiN particles present in the Ti–V steels, which were designed for RCR processing.[20] However, when finish rolling begins *above* the T_{nr}, the relatively coarse austenite grains present after roughing are replaced by fine dynamically recrystallized grains (Fig. 12(a)). By contrast, when finish rolling begins *below* the T_{nr}, the coarse austenite grains remain, but are severely pancaked (Fig. 12(b)).

The austenite microstructures in Figs. 12(a) and 12(b) transform to similar ferrite grain sizes: 6.2 and 5.9 μm (Figs. 12(c) and 12(d), respectively). The number of ferrite nucleation sites in the austenites depicted in Figs. 12(a) and 12(b) are therefore expected to be similar. Thus, in contrast to the observations described above for the Ti–V steels, where significant ferrite grain refinement was produced by lowering the finish rolling temperature (Fig. 7), this process variation does not lead to grain refinement in the Nb–V steel. Clearly, during SRM simulation, alloys specifically designed for RCR rolling are also suitable for DRCR rolling in that they permit optimization of the ferrite grain refinement by decreasing the finish rolling temperature.

4. Discussion

As described above, in the Ti–V steels designed for RCR rolling, the grain refinement brought about by DRCR can be optimized by decreasing the SRM exit temperature to the vicinity of the A_{r3}. However, in the more highly alloyed 19C–01Ti–15V grade, the DRCR process was taken beyond its limit with regard to decreasing the finish rolling temperature, as indicated by the strain that accumulated during the last few passes. Such strain accumulation appears to have started when dynamic recrystallization was already well under way. By contrast, in the Nb–V steel designed for CCR, grain refinement by DRCR only occurred at the *higher* finish rolling temperature. When SRM rolling was initiated well below the T_{nr},

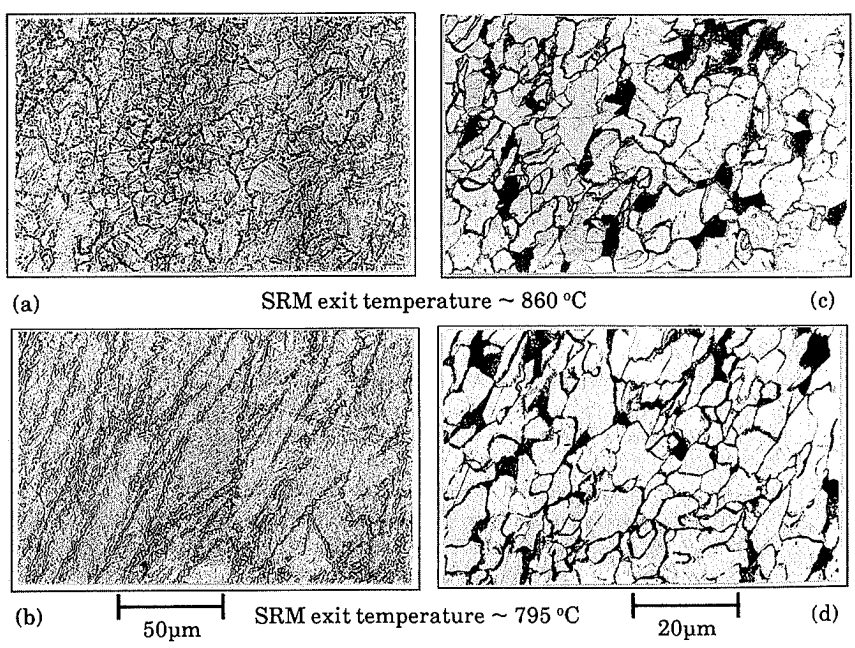

Fig. 12.
Austenite microstructures (a) and (b), immediately after the SRM simulations displayed in Fig. 10, and the corresponding room temperature microstructures (c) and (d).
Note that austenite pancaking occurs when the finish rolling temperature is decreased from 860 to 795°C and that this has little effect on the ferrite grain size.

pancaking of the relatively coarse austenite grains present after roughing took place.

Further reductions in the finish rolling temperature are unlikely to lead to further refinements in the ferrite grain size, as long as the same total strain is being applied and the austenite is being pancaked to the same degree. By contrast, in the DRCR process, which takes place in the Ti–V steels, the austenite grain size decreases with finish rolling temperature, consequently reducing the ferrite grain size. This leads to the general conclusion that, by decreasing the finish rolling temperature, dynamic recrystallization can produce finer ferrite grain sizes than can be achieved by pancaking.[4]

In order for carbonitride precipitation to take place in the austenite during SRM rolling, the rate of precipitation must be very rapid because of the short interpass delays (0.5 s), as well as the relatively short times the steel is held below the T_{nr} in this schedule. Some typical strain-induced precipitation start times (P_s) for Nb(CN) are displayed in relation to the time available for such precipitation during SRM rolling in Fig. 13(a). These are the P_s times which are expected to apply under continuous-cooling-precipitation (CCP) conditions; they are shown as a function of the time elapsed from the first pass. The continuous cooling curve associated with an SRM entry temperature of 910°C indicates that the strain-induced precipitation of Nb(CN) begins at an early stage (the 6th pass) in the Nb–V steel, so that dynamic recrystallization is prevented, and pancaking takes place instead. By contrast, when SRM rolling is initiated at 1 000°C, (uppermost curve), strain-induced precipitation is only nucleated near the exit of the SRM, by which time the DRCR process is already well under way, thus limiting the extent of pancaking.

It is well known that the noses of PTT curves for V-bearing steels are located at lower temperatures than those of Nb-bearing steels.[19,23] An expected CCP curve for VN precipitation is also illustrated in Fig. 13(a). Here it can be seen that, for the same SRM entry temperature of 910°C, the continuous cooling curve intersects the CCP curve for VN precipitation only after the 16th pass. When the SRM entry temperature is 850°C, on the other hand, precipitation will begin at the 13th pass, as in the Nb–V steel when the entry temperature of 1 000°C is employed. It is apparent from these examples that, for DRCR processing, there should be no strain-induced precipitation at all during processing, as in the case of the 910°C rolling of the V steel. Thus, whereas CCR schedules are intended to pass through the nose of the CCP curve, DRCR schedules, on the other hand, should aim at avoiding the nose entirely.

The above approach can assist in the design of CCR and DRCR schedules with respect to various candidate steels and processes. In plate and reversing mill schedules, for example, the interpass delays are quite long, so that the continuous cooling curves are likely to intersect the CCP curve during the early stages of rolling. A schedule of this type is illustrated in Fig. 13(b), where it can be seen that most of the CCR passes are applied in the strain-induced precipitation zone. By contrast, in the SRM schedule (or in other schedules of the tandem mill type), the interpass delays are more than an order of magnitude shorter. Hence rolling can be designed to finish before the start of strain-induced precipitation, as indicated

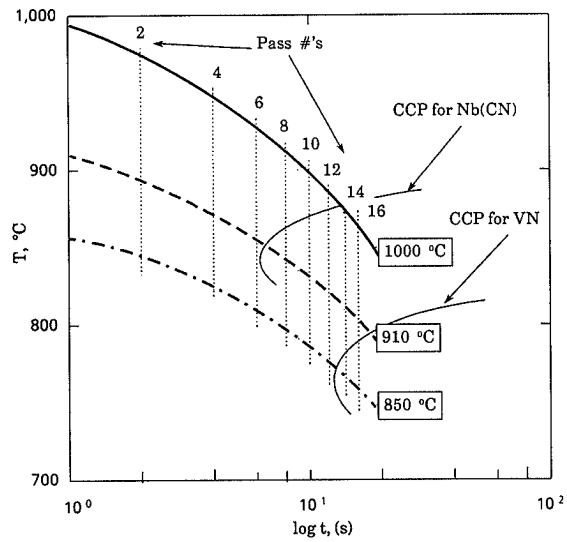

Fig. 13(a). The continuous cooling curves associated with SRM entry temperatures of 1 000, 910 and 850°C shown as a function of the time elapsed from the first pass of SRM rolling.
The latter indicates the time available for strain-induced precipitation up to the pass number identified by the respective dotted vertical line.
Also shown are the expected P_s times for the strain-induced precipitation of Nb(CN) and VN under continuous cooling conditions (CCP curves).

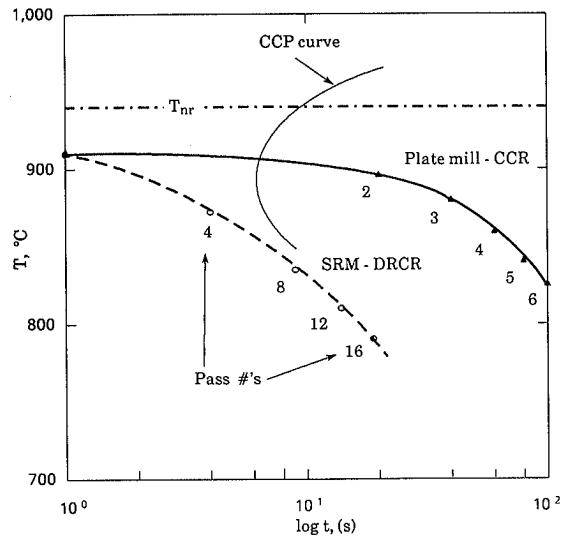

Fig. 13(b). The continuous cooling curves associated with an SRM (DRCR) schedule and a typical plate mill (CCR) schedule shown as a function of the time elapsed from the first pass of finish rolling.
The abscissa indicates the time available for strain-induced precipitation up to the respective pass number.
A typical P_s curve for strain-induced precipitation under continuous cooling conditions (CCP curve) is also shown.

in Fig. 13(a) for the Ti–V steel, where the SRM entry temperature is 910°C and the cooling curve intersects the CCP curve *above* the nose. Alternatively, when finish rolling thin products such as strip, the associated faster cooling rate can avoid the nose of the P_s curve by passing *below* it, as shown in Fig. 13(b). Once again, under these conditions, precipitation will not take place during rolling, and DRCR schedules can be safely employed.

5. Conclusions

This research was carried out with the aim of optimizing the ferrite grain refinement that can be achieved by DRCR. A seamless tube hot forming process was simulated by means of torsion testing, with particular attention being paid to the stretch reducing mill (SRM).[5] A simplified plate schedule, representing reversing mills which produce pancaking at low finishing temperatures, was also studied to compare CCR with DRCR. For the Ti–V steels, the above work led to the following conclusions.

(1) When the simplified plate schedule, with 20 s interpass delays, was employed, the passes applied below the no-recrystallization temperature or T_{nr} produced austenite pancaking and considerable retained work hardening.

(2) By contrast, when the total deformation was applied below the T_{nr}, in the absence of static recrystallization during the short (0.5 s) interpass delays, strain was accumulated in the early passes. At larger strains, dynamic recrystallization was initiated due to the absence of strain-induced precipitation. This is because the SRM cooling curve only intersects the CCP (continuous-cooling-precipitation) P_s curve at the last few passes. Thus the short interpass times lead to *lower* resistances to hot deformation than when reversing mill schedules are employed.

(3) The early stages of strain accumulation can be readily followed by examining the austenite microstructures in quenched specimens. Similar remarks apply to the progress of dynamic recrystallization after its initiation, which progressively consumes the pancaked grains, leading to the development of a fine dynamically recrystallized austenite microstructure. The grain refinement produced by dynamic recrystallization can be optimized by reducing the SRM entry temperature. Decreasing the SRM exit temperature from 860 to about 740°C refines the ferrite grain size from 6.6 to 3.3 μm and from 7.7 to 4.7 μm for the 19C–01Ti–15V and 10C–01Ti–10V grades, respectively. For both steels, the grain refinement produced by this method is at its limit when the SRM exit temperature corresponds to the A_{r3}.

(4) The strain necessary to initiate dynamic recrystallization is raised when the SRM entry temperature is reduced, leading to higher MFS's.

For the Nb–V steels, the major conclusions were the following:

(1) During SRM rolling, when the entry temperature is above the T_{nr}, the dynamic recrystallization behavior is similar to that of the Ti–V steels; strain accumulation in the early stages is followed by dynamic recrystallization. However, when the SRM entry temperature is reduced to below the T_{nr}, and the SRM cooling curve passes through the nose of the CCP curve, the strain continues to accumulate, leading to austenite pancaking.

(2) The fine austenite grains produced by dynamic recrystallization at the higher temperatures of finish rolling and the coarse pancaked grains obtained after lower temperature finishing both transform to similar ferrite grain sizes. Thus for this steel, lowering the finish rolling temperature does not lead to a reduction in the ferrite grain size.

Acknowledgments

The authors are indebted to the Algoma Steel Corporation for permission to publish this work. They also acknowledge with gratitude the financial assistance received from the Canadian Steel Industry Research Association, the Natural Sciences and Engineering Research Council of Canada, and the Quebec Ministry of Education (FCAR program). Thanks are also due to Dr. S. Yue (McGill University), Mr. P. J. Hunt (Algoma Steel Corporation) and Dr. G. E. Ruddle (MTL, CANMET) for many helpful discussions, and to Mr. P. D. Hodgson (BHP, Australia) for comments on the manuscript. The steels were supplied by MTL, CANMET and Algoma.

REFERENCES

1) I. Tamura: Proc. Int. Conf. on Physical Metallurgy of Thermomechanical Processing of Steels and Other Metals (THERMEC-88), I. Tamura, ed., ISIJ, Tokyo, (1988), 1.
2) B. Dogan, L. E. Collins and J. D. Boyd: *Metall. Trans. A*, **19A** (1988), 1221.
3) F. H. Samuel, S. Yue, J. J. Jonas and B. A. Zbinden: *ISIJ Int.*, **29** (1989), 878.
4) F. H. Samuel, S. Yue, J. J. Jonas and K. R. Barnes: *ISIJ Int.*, **30** (1990), 216.
5) L. N. Pussegoda, S. Yue and J. J. Jonas: *Metall. Trans. A.*, **21A** (1990), 153.
6) G. E. Ruddle, D. L. Baragar and A. F. Crawley: 26th Mechanical Working and Steel Processing Conf. Proc., Vol. XXII, ISS-AIME, Warrendale, PA, (1984), 183.
7) F. Boratto, S. Yue and J. J. Jonas: United States Patent No. 4,840,051 (June 20, 1989).
8) P. Choquet, A. Le Bon and Ch. Perdrix: Strength of Metals and Alloys, ed. by H. J. McQueen, J.-P. Bailon, J. I. Dickson, J. J. Jonas and M. G. Akben, Pergamon Press, Oxford, (1985), 1025.
9) B. Migaud: Hot Working and Forming Processes, ed. by C. M. Sellars and G. J. Davies, Met. Soc., London, (1980), 67.
10) L. N. Pussegoda, R. Barbosa, S. Yue, J. J. Jonas and P. J. Hunt: *J. Mater. Processing Technol.*, (1991), in press.
11) T. Chandra, S. Yue and J. J. Jonas: Proc. Conf. on the Science and Technology of Flat Rolling, Deauville, France, (1987), F18.1.
12) S. Yue, F. Boratto and J. J. Jonas: Proc. Conf. on Hot and Cold-Rolled Sheet Steels, ed. by R. Pradhan and G. Ludkovsky, TMS-AIME, Warrendale, PA, (1988), 349.
13) S. L. Semiatin, G. D. Lahoti and J. J. Jonas: ASM Metals Handbook, Vol. 8 (Mechanical Testing), 9th Ed., ASM, Metals Park, OH, (1985), 154.
14) F. H. Samuel, S. Yue, and J. J. Jonas: Proc. Recrystalliza-

tion '90, IMMA, Australia, (1990), 325.
15) S. S. Hansen, J. B. Vander Sande and M. Cohen: *Metall. Trans. A*, **11A** (1980), 387.
16) K. J. Irvine, F. B. Pickering and T. Gladman: *J. Iron Steel Inst.*, **205** (1967), 161.
17) T. Sakai, M. Ohashi, K. Chiba and J. J. Jonas: *Acta metall.*, **36** (1988), 1781.
18) R. A. Petkovic, M. J. Luton and J. J. Jonas: *Can. Metall. Quart.*, **14** (1975), 137.
19) M. J. Crooks, A. J. Garratt-Reed, J. B. Vander Sande and W. S. Owen: *Metall. Trans. A*, **12A** (1981), 1999.
20) L. N. Pussegoda, S. Yue and J. J. Jonas: *Mater. Sci. Technol.*, (1991), in press.
21) T. Siwecki: Proc. Int. Conf. on Physical Metallurgy of Thermomechanical Processing of Steels and Other Metals (THERMEC-88), I. Tamura, ed., ISIJ, Tokyo, (1988), 232.
22) C. M. Sellars and J. H. Beynon: High Strength Low Alloy Steels, ed. by D. P. Dunne and T. Chandra, Univ. of Wollongong, Wollongong, NSW, (1985), 142.
23) M. G. Akben, I. Weiss and J. J. Jonas: *Acta metall.*, **29** (1981), 111.